

# **Experimental Investigation of Relative Permeability Upscaling from the Micro-Scale to the Macro-Scale**

**Semi-Annual Progress Report**

**Reporting Period Start Date: March 1, 2000**

**Reporting Period End Date: August 31, 2000**

**Laura J. Pyrak-Nolte, Ping Yu, Jiangtao Cheng and Nicholas Giordano**

**December 2000**

**DOE Award: DE-AC26-99BC15207**

**Purdue Research Foundation  
Department of Physics  
1396 Physics Building, Room 166  
West Lafayette, Indiana 47907-1396**

**Disclaimer:** This report was prepared as an account of the work sponsored by an agency of the United States Government. Neither the United States Government nor any agency thereof, nor any of their employees, makes any warranty, express or implied, or assumes any legal liability or responsibility for the accuracy, completeness, or usefulness of any information, apparatus, product, or process disclosed, or represents that its use would not infringe privately owned rights. Reference herein to any specific commercial product, process, or service by trade name, trademark, manufacturer, or otherwise does not necessarily constitute or imply its endorsement, recommendation, or favoring by the United States Government or any agency thereof. The views and opinions of the authors expressed herein do not necessarily state or reflect those of the United States Government or any agency thereof.

**Abstract:** The principal challenge of upscaling techniques for multi-phase fluid dynamics in porous media is to determine which properties on the micro-scale can be used to predict macroscopic flow and spatial distribution of phases at core- and field-scales. The most notable outcome of recent theories is the identification of interfacial areas per volume for multiple phases as a fundamental parameter that determines much of the multi-phase properties of the porous medium. A formal program of experimental research was begun to directly test upscaling theories in fluid flow through porous media by comparing measurements of relative permeability and capillary-saturation with measurements of interfacial area per volume. During this reporting period, work was performed to initial test the laboratory equipment that will be used for testing the upscaling theories and to provide initial data sets. The holographic laser imaging technique (Optical Coherence Imaging) underwent initial testing and provided initial results (on imaging through turbid media, three-dimensional laser ranging and imaging sandstone), which lead to modifications to the system. Initial testing of the relative permeability system for the laboratory micro-models was performed and provided initial results on drainage & imbibition experiments. Initial testing of the Wood's metal injection system and permeability measurement system was performed on sandstone cores and modification to the system were made.

## Table of Contents

<b>Title Page</b>	
<b>Disclaimer</b> .....	i
<b>Abstract</b> .....	ii
<b>Table of Contents</b> .....	iii
<b>List of Figures</b> .....	iv
<b>Executive Summary</b> .....	1
<b>1.0 Introduction</b> .....	2
1.1 SUMMARY OF PROJECT DESCRIPTION.....	2
1.2 PROJECT OBJECTIVES.....	4
<b>2.0 Results and Discussion by Task</b> .....	5
2.1 TASK 1. CONSTRUCTION OF EQUIPMENT AND INITIAL TESTING.....	5
2.1.1 <i>Task 1a Optical Coherence Imaging</i> .....	5
2.1.2 <i>Task 1c Adaptation of the Micro-Model System for Multiphase Flow Measurements</i> .....	13
2.1.3 <i>Task 1d Relative Permeability/Wood’s Metal Injection System</i>	14
2.2 TASK 2 SAMPLE PREPARATION.....	19
2.2.1 <i>Task 2a Photorefractive Quantum Well Devices (PRQW)</i> .....	19
2.2.2 <i>Task 2b Core Samples and Boreholes</i> .....	20
2.2.3 <i>Task 2c Fabrication of Micromodels</i> .....	22
2.3 TASK 3 MEASUREMENTS OF INTERFACIAL AREA AND PORE GEOMETRY.....	24
2.3.1 <i>Task 3a Pore Geometry and Optical Coherence Imaging (OCI)</i> ...	24
2.3.2 <i>Task 3b Interfacial area, pore geometry and hydraulic properties from micro-models</i> .....	24
2.3.3 <i>Task 3c Interfacial area, pore geometry and hydraulic measurements on Core sample</i> .....	29
<b>3.0 Conclusions and Future Work</b> .....	31
3.1 OPTICAL COHERENCE IMAGING.....	31
3.2 MICRO-MODELS.....	32
3.3 WOOD’S METAL INJECTION.....	33
<b>4.0 References</b> .....	34

## List of Figures

Figure 1. Setup of optical coherence imaging. The red lines represent the modified setup and the dash lines are from original setup.....	6
Figure 2. USAF test chart labeled with the sizes of the bars.....	7
Figure 3. Direct image (a) and hologram (b) of USAF test chart. In the hologram, the minimum bar that can be resolved is element 5 at group 5. The full area of the picture represents $3 \times 2 \text{ mm}^2$ on the sample plane.....	8
Figure 4. Direct image and hologram of the USAF test chart through 6 MFP of turbid medium. The minimum resolved bar is from element 5 at group 4, which shows the system resolution of $20 \text{ }\mu\text{m}$ .....	9
Figure 5. Holograms show ability of optical coherence imaging on different depths of 3D test object. The depth step is $200 \text{ }\mu\text{m}$ . The ring diameter increases with each $250 \text{ }\mu\text{m}$ . Please notice that large rings are cut off by PRQW device that has size of $1.0 \text{ mm}$ in width.....	11
Figure 6. Holograms show 3D imaging through 3-MFP turbid medium. Other conditions are the same as figure 5.....	12
Figure 7. Sketch of apparatus for measuring and imaging multiphase flow in micro-model samples.....	13
Figure 8 New design of the inlet and outlet with a control channel added.....	15
Figure 9. Schematic of Wood's metal injection system and permeability measurement system.....	18
Figure 10. Holograms of the USAF test chart using a new PRQW device.....	19
Figure 11. Sample density and porosity as function of sample size.....	20
Figure 12. One tier mask used to make fractal structures.....	23
Figure 13. Five tier mask used to make fractal structures that are spatially correlated	23

Figure 14. Direct image (a) and hologram (b) of polished sandstone. The hologram has a size of 1.0x1.5 mm <sup>2</sup> and resolution of 10 μm. The white region corresponds to grains which are 30-50 μm in size.....	25
Figure 15. Using the mask shown in Figure 12, we made a micro-model with this percolation geometry. The pattern was taken in red light to prevent unwanted photochemical reactions in the photoresist layer in which the pattern is etched. The region shown here is 600 micron long and wide. The darker area is photoresist, and the brighter area is void space.....	27
Figure 16. A fractal micro-model filled with silicone oil and nitrogen gas. The brightest region is gas and the darker regions show the space filled with silicone oil and the inaccessible regions (compare with Figure 15, which shows the same micro-model with an empty void space).....	27
Figure 17. Drainage and imbibition curve for silicone oil / nitrogen gas in the micro-model shown in Figure 16. The horizontal axis gives the fraction of the available pore area which is occupied by the wetting phase (oil).....	28
Figure 18. Flow rate versus gas pressure during gas permeability measurement .....	29
Figure 19. Water flow rate versus gas pressure during gas permeability measurement for Run 1 and Run 2. Units are converted and the slope of the fitted line is the permeability in unit of L/T <sup>2</sup> .....	30
Figure 20. Image of Wood's metal injected sandstone obtained using an optical microscope.....	32

## List of Tables

Table 1. The line width (in $\mu\text{m}$ ) of the bars of USAF test chart in different groups and element numbers .....	7
Table 2. Comparison between gas porosimeter and wet/dry porosity.....	21
Table 3. Comparison of sample porosity before and after epoxy coating .....	22
Table 4. Properties of Silicone oil.....	26

## **Executive Summary**

Direct experimental tests of upscaling theories in fluid flow through porous media will be made by comparing measurements of relative permeability and capillary-saturation with measurements of interfacial area per volume. These experiments are performed from microns at the pore-scale to centimeters at the core-scale, spanning four orders of magnitude in size. Three objectives provide the data for rigorous experimental tests of upscaling theories. First, holographic laser imaging techniques will acquire pore-scale three-dimensional optical images of the pore geometry in reservoir sandstones. This technique uses unique properties of coherent light to see through drilling muds and into the sandstone. Second, laboratory micro-models with matched topological properties based on the data from the pore imaging will make it possible to measure interfacial area per volume in scientifically controlled imbibition and drainage experiments, combined with measurements of capillary-pressure-saturation data and relative permeability. Third, core-scale experiments of relative permeability and capillary-saturation, and metal casts of the pore geometry, will be compared with the pore-scale data of the first two objectives. The data from all these objectives will provide the first complete picture over such a large dynamic range. It will make it possible to answer the principal question concerning flow upscaling: which microscopic measurements are most useful for predicting macroscopic flow properties of an oil reservoir. The tangible outcome of this work will be explicit data connecting interfacial areas, or other relevant geometric micro-scale data, with macroscopic hydraulic properties. In addition, we show strong industrial interest in testing and commercializing the unique down-hole laser imaging technology that can be transferred to the oil-industry service-company sector.

During this reporting period, work was performed to initial test the laboratory equipment that will be used for testing the upscaling theories and to provide initial data sets. The holographic laser imaging technique (Optical Coherence Imaging) underwent initial testing and provided initial results (on imaging through turbid media, three-dimensional laser ranging and imaging sandstone), which lead to modifications to the system. Initial testing of the relative permeability system for the laboratory micro-models was performed and provided initial results on drainage & imbibition experiments. Initial testing of the Wood's metal injection system and permeability measurement system was performed on sandstone cores and modification to the system were made.

## 1.0 Introduction

### 1.1 SUMMARY OF PROJECT DESCRIPTION

Standard expressions of multi-phase flow in porous media based on modifications of Darcy's Law (Darcy, 1856) have crippling deficiencies that make them undesirable to use for critical operations such as tertiary recovery of oil from depleted reservoirs. The primary difficulty in these empirical expressions are their violation of rigorous conservation laws. New theories based on rigorous volume averaging theorems and fundamental thermodynamic principles of phase boundaries have emerged in the past decade to replace the old empirical rules (Hassanizadeh and Gray, 1979; Gray, 1983; Kalaydjian, 1990). The most notable outcome of these theories is the identification of interfacial areas per volume for multiple phases as fundamental parameters that determine much of the multi-phase properties of the porous medium (Muccino, Gray and Ferrand, 1998).

Interfacial areas per volume provide natural descriptions of fundamental physical processes in porous media. For instance, thermodynamic energies are proportional to interfacial areas, and interfacial areas per volume represent a form of energy density. Gradients in energy densities define the dynamical pressures that drive the movement and distribution of phases within a complex topology. Interfacial areas per volume in a porous medium therefore represent a three-dimensional potential energy landscape.

Interfacial areas per volume also provide a natural yard-stick for defining the role of scale in multiphase fluid properties. The dimensional units of interfacial area per volume is a spatial frequency (inverse length) that breaks scale invariance. A useful illustration (Gray, 1998) of this scale-defining role can be made by considering an image of a pore-geometry containing only a single phase. Without a measurement scale, it is impossible to state what the physical size of the system is. However, when two phases such as water and air are both present, the length scale becomes obvious. At small scales, the water-air interface is drawn into the pore throats, while at large scales the water puddles in the large void volumes.

Therefore, the interfacial areas between phases define a length scale. Whenever a physical system has an intrinsic length scale, the physics of the system can be divided into two regimes: one where sample sizes are larger than the intrinsic length scale, and the other where information is obtained on scales smaller than the intrinsic length scale. Breaking scale invariance makes it possible to define representative elementary volumes (REV) and to apply averaging theorems. Combining the averaging theorems with thermodynamics further constrains the possible types of constitutive equations that can rigorously describe multiphase fluid properties in porous media.

As a consequence of this theoretical framework, interfacial areas per volume (IAV) take on a more important role than simple volume saturation. This important role of IAV is clear because a single value of relative volume saturation can correspond to infinitely different distributions of two phases within the volume. Large values of IAV relate to a finely distributed phase that can block pore throats and seriously affect permeability, while small values of IAV relate to gross separations of phases, with large connected volumes of the phase that can flow unimpeded through the network. Significant numerical studies have been performed on the relationships between capillary-saturation and interfacial area. Reeves and Celia (1995) developed a numerical model that scans over repetitive imbibition and drainage while tracking the interfacial area for each loop. These studies pointed to a non-unique relationship between interfacial area and partial saturation, although a family of curves did emerge that lies within a localized part of the parameter space defined by area and saturation.

The numerical studies illustrate the importance of continued and extensive experimental studies and tests of upscaling theories, and in particular tests of the role of interfacial area per volume in determining macroscopic flow properties. While oil recovery predictions should certainly include IAV as critical parameters, it is important to test whether other microscopic parameters also contribute to the macroscopic behavior. For instance, scale invariance of interfacial areas, even over restricted length scales, could present serious challenges to the averaging theorems, and could modify the presumed role of interfacial area in determining

macroscopic flow properties. The principal objective of our proposed upscaling approach is to experimentally measure many microscopic geometric parameters of the flow system over many scales, and connect these microscopic measurements with macroscopic flow behavior.

## 1.2 PROJECT OBJECTIVES

The proposed work for this contract has three objectives that will provide rigorous experimental tests of upscaling theories. The objectives are:

1) To use holographic laser imaging techniques to acquire pore-scale three-dimensional optical images of the pore geometry in reservoir sandstones. This technique uses unique properties of coherent light to see through drilling muds and up to a millimeter into the sandstone. This data forms the basis of upscaling experiments to test theories of interfacial area per volume.

2) To construct laboratory micro-models with matched topological properties based on the data from the pore imaging. Interfacial area per volume will be measured directly in controlled imbibition and drainage experiments, together with capillary-pressure-saturation data and relative permeability data. This set of interrelated data will allow rigorous testing of upscaling theories.

3) To perform core-scale experiments of relative permeability and capillary-saturation, and to make metal casts of the pore geometry and interfacial area per volume. This core-scale data (including pore-scale from the metal casts) will be compared with the pore-scale data of the first two objectives, extending the observation scales over four orders of magnitude.

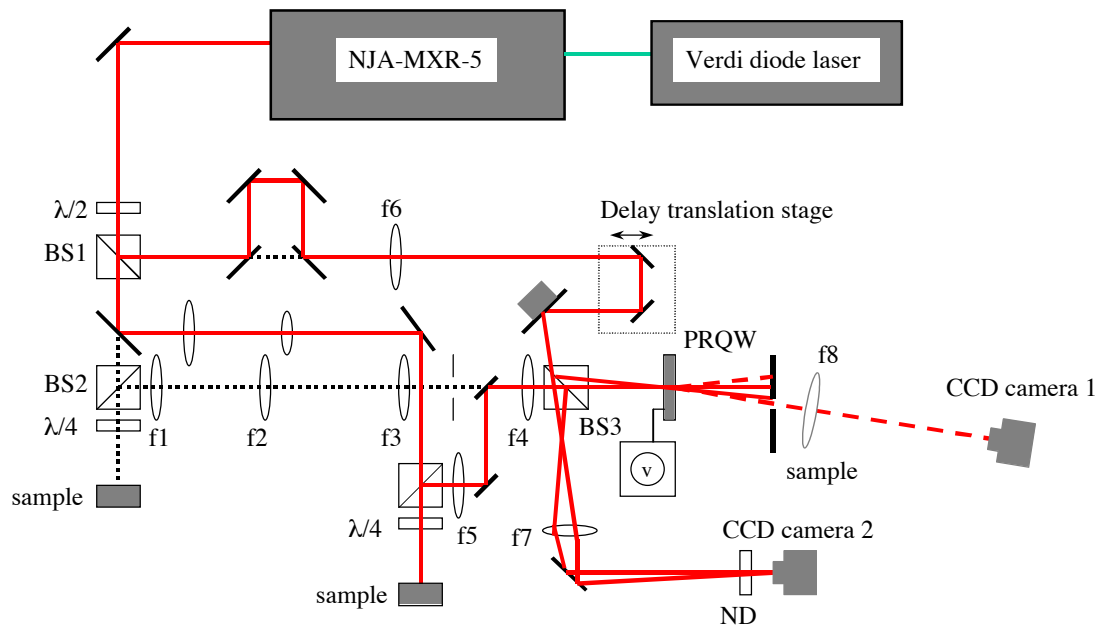
## 2.0 Results and Discussion by Task

### 2.1 TASK 1. CONSTRUCTION OF EQUIPMENT AND INITIAL TESTING

An objective of this project is to directly test through experimental measurements upscaling theories for fluid flow through porous media by comparing measurements of relative permeability and capillary-saturation with measurements of interfacial area per volume. The three experimental approaches each require initial testing and modifications to improve system performance. The main results for this report period consist of the initial testing of the equipment and the modification of equipment to improve performance.

#### 2.1.1 Task 1a *Optical Coherence Imaging*

During this reporting period, two modifications to the optical coherence imaging system were made. Figure 1 shows the revised optical set-up that improves the resolution of the optical coherence imaging system and the intensity of the detected image. The intensity of the detected image was increased by decreasing the diameter (3.0 mm) of pump beam by using a telescope that consists of two lenses with focus length ratio of 4:1. This increases the intensity of the detected image by 16. To improve the resolution of the optical coherence imaging system, the magnification of the imaging system was modified by using two 150 mm lenses ( $f_4$  and  $f_5$  in fig. 1). The new lens resulted in holograms with a resolution of 10  $\mu\text{m}$  in both horizontal and vertical directions, which is only limited by the PRQW device.



BS1, BS2: polarization beam splitter. BS3: 50/50 beam splitter.  
 $f_1=200\text{mm}$ ,  $f_2=100\text{mm}$ ,  $f_3=150\text{mm}$ ,  $f_4=f_5=150\text{mm}$ ,  $f_6=500\text{mm}$ ,  $f_7=50\text{mm}$ ,  $f_8=150\text{mm}$ .  
 ND: Neutral Density Filter

Figure 1. Setup of optical coherence imaging. The red lines represent the modified setup and the dash lines are from original setup.

To test the resolution of the OCI system, the United States Air Force (USAF) test chart is used as the control image because it has calibrated bars of varying sizes. A typical image of the USAF test chart is shown in Figure 2 and the sizes of the bars are listed in Table 1. Figure 3(a) is a direct image recorded by the CCD camera 2 in Figure 1 using the femtosecond laser (center wavelength of 838 nm and bandwidth of 12 nm). The hologram of the test chart in figure 3(b) shows the bar of element 5 at group 5 can be resolved, which

means the system resolution is  $10\ \mu\text{m}$ . In figure 3, the size of the hologram is 1.0 mm in diameter and is limited by the finite size of the beam.

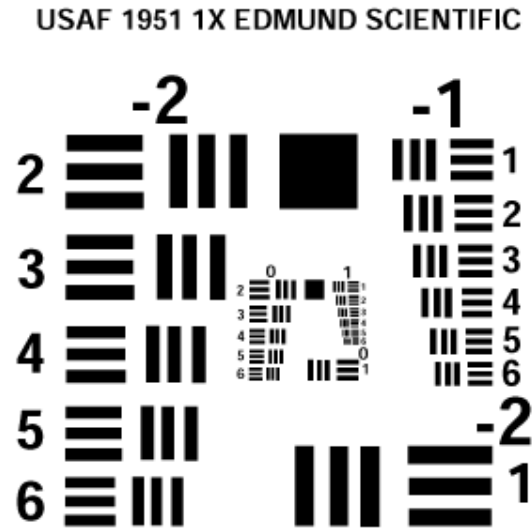
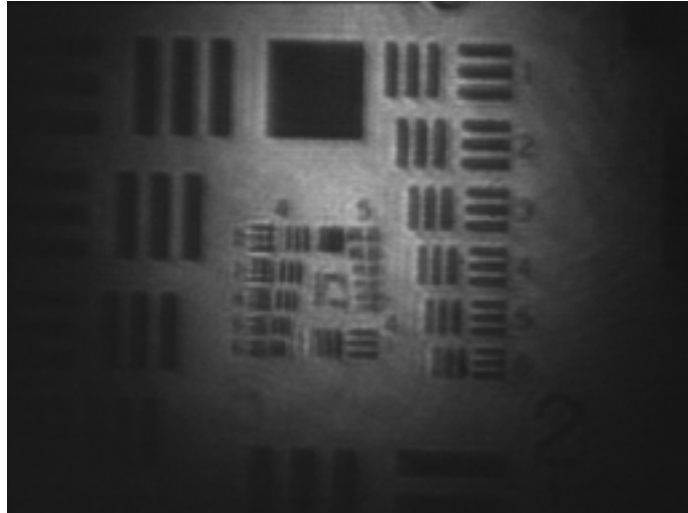


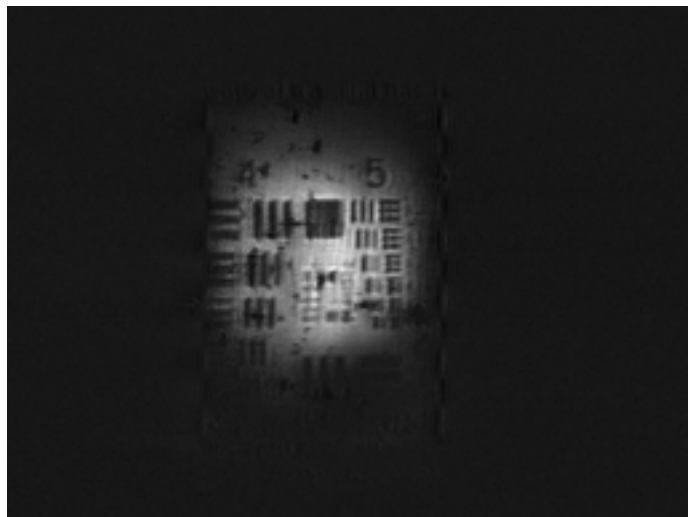
Figure 2. USAF test chart labeled with the sizes of the bars.

Table 1. The line width (in  $\mu\text{m}$ ) of the bars of USAF test chart in different groups and element numbers.

<i>Element No.</i>	<b>Group No.</b>							
	<b>0</b>	<b>1</b>	<b>2</b>	<b>3</b>	<b>4</b>	<b>5</b>	<b>6</b>	<b>7</b>
<b>1</b>	500	250	125	62.5	31.25	15.63	7.81	3.91
<b>2</b>	446.43	223.21	111.36	55.68	27.86	13.89	6.96	3.47
<b>3</b>	396.83	198.41	99.21	49.50	24.80	12.41	6.20	3.11
<b>4</b>	354.61	176.68	88.34	44.25	22.10	11.04	5.52	2.76
<b>5</b>	314.47	157.73	78.74	39.37	19.69	9.84	4.90	2.46
<b>6</b>	280.90	140.45	70.13	34.97	17.54	8.77	4.39	2.19



(a)



(b)

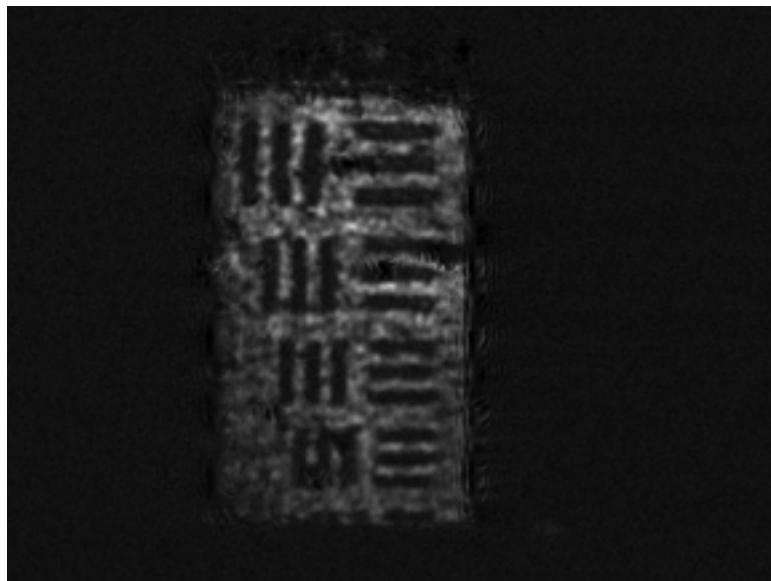
Figure 3. Direct image (a) and hologram (b) of USAF test chart. In the hologram, the minimum bar that can be resolved is element 5 at group 5. The full area of the picture represents  $3 \times 2 \text{ mm}^2$  on the sample plane. *(See electronic version for higher image quality)*

Initial testing was performed to determine the ability of the OCI system to image through turbid medium. This is an important test because a potential application of OCI is to image through drilling fluids that often has clay particles in suspension, i.e., a turbid medium. The USAF test chart was imaged in reflection with the OCI system through a cuvette (optically flat cubic glass cell) filled with a scattering medium, i.e., distill water and polystyrene

microspheres. The solution corresponds to approximately 6-mfp (mean free paths) scattering depth in double pass.



(a)



(b)

Figure 4. (a) Direct image and (b) hologram of the USAF test chart through 6 MFP of turbid medium. The minimum resolved bar is from element 5 at group 4, which shows the system resolution of 20  $\mu\text{m}$ . (*See electronic version for higher image quality*)

Fig.4(a) shows the image of the test chart when view directly through the scattering medium by the CCD camera. The image is totally obscured by the scattering of light. Fig.4(b) is the hologram from photorefractive quantum well device (PRQW) by degenerate four wave mixing method, i.e., from the OCI system. The smallest observable bars are on the order of 20  $\mu\text{m}$ . The experiment demonstrates the ability of OCI (photorefractive holography of PRQW) to discriminate against the incoherent background light and the ability to image through a turbid medium.

Initial testing of the OCI systems ability to capture three-dimensional (3-D) information (i.e., laser ranging) from an object was also tested. An aluminum test object was fabricated that is cylindrical in shape with a series of 200  $\mu\text{m}$  steps that were machined into one end of the cylinder. The depth resolution of the system is limited by the coherence length of the femtosecond laser, which is 30  $\mu\text{m}$  at the wavelength bandwidth of 12 nm. By imaging a 3-D object that consisted of a set of cylindrical steps, the depth resolved holograms are demonstrated (Figure 5). In Figure 5, a series of images of annular rings are shown. The different rings were acquired by adjusting the delay in the reference arm of the OCI system, which correspond to different steps of the 3D object. In addition, measurements were performed to test laser ranging through a turbid medium using the OCI system. Figure 6 shows the holograms that were acquired for the 3D object through a 3-mfp (mean free path) turbid medium that was placed in front of the object. This demonstrates the ability to perform laser ranging of object inside turbid medium.

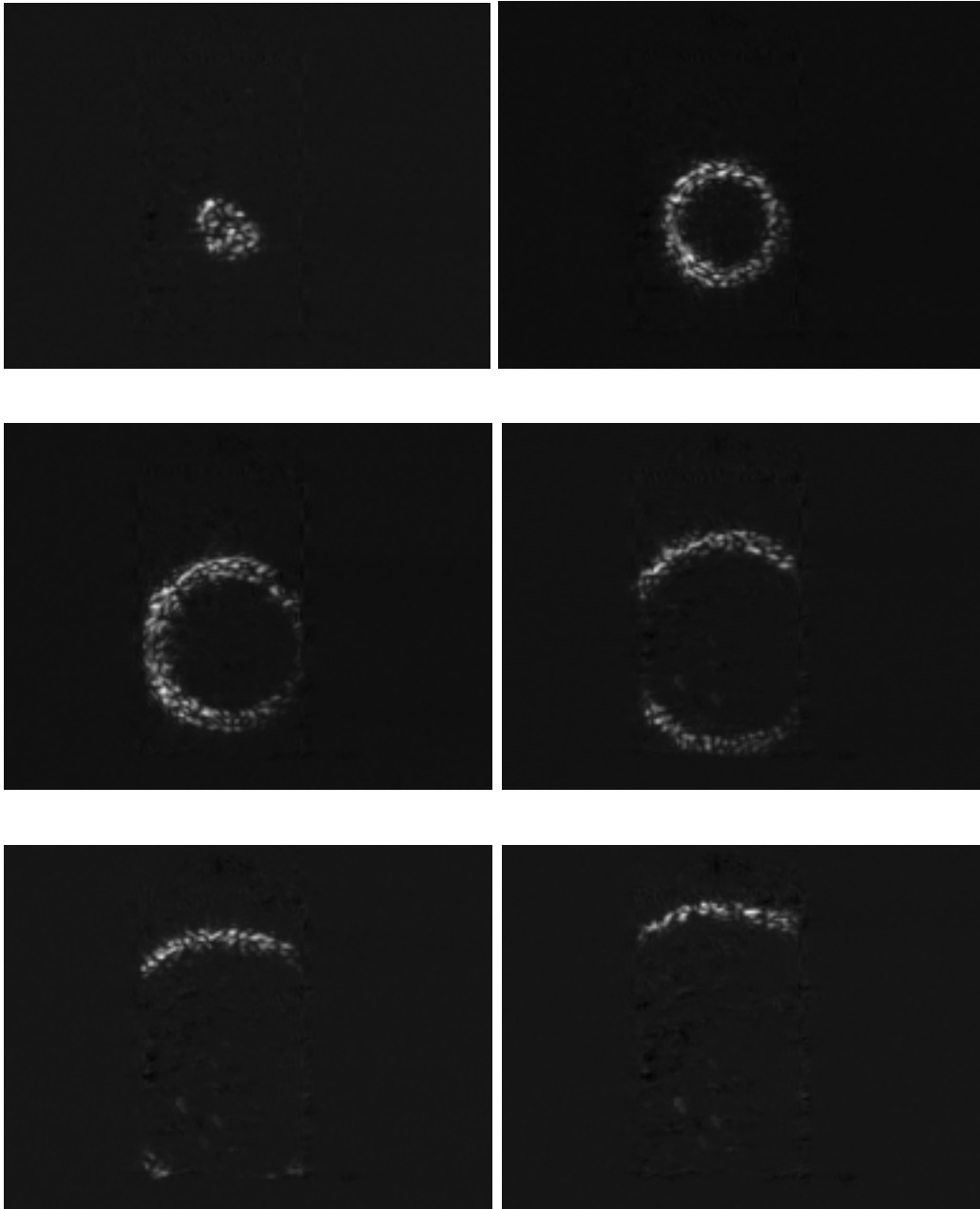


Figure 5. Holograms show ability of optical coherence imaging on different depths of 3D test object. The depth step is 200  $\mu\text{m}$ . The ring diameter increases with each 250  $\mu\text{m}$ . Please notice that large rings are cut off by PRQW device that has size of 1.0 mm in width. (*See electronic version for higher image quality*)

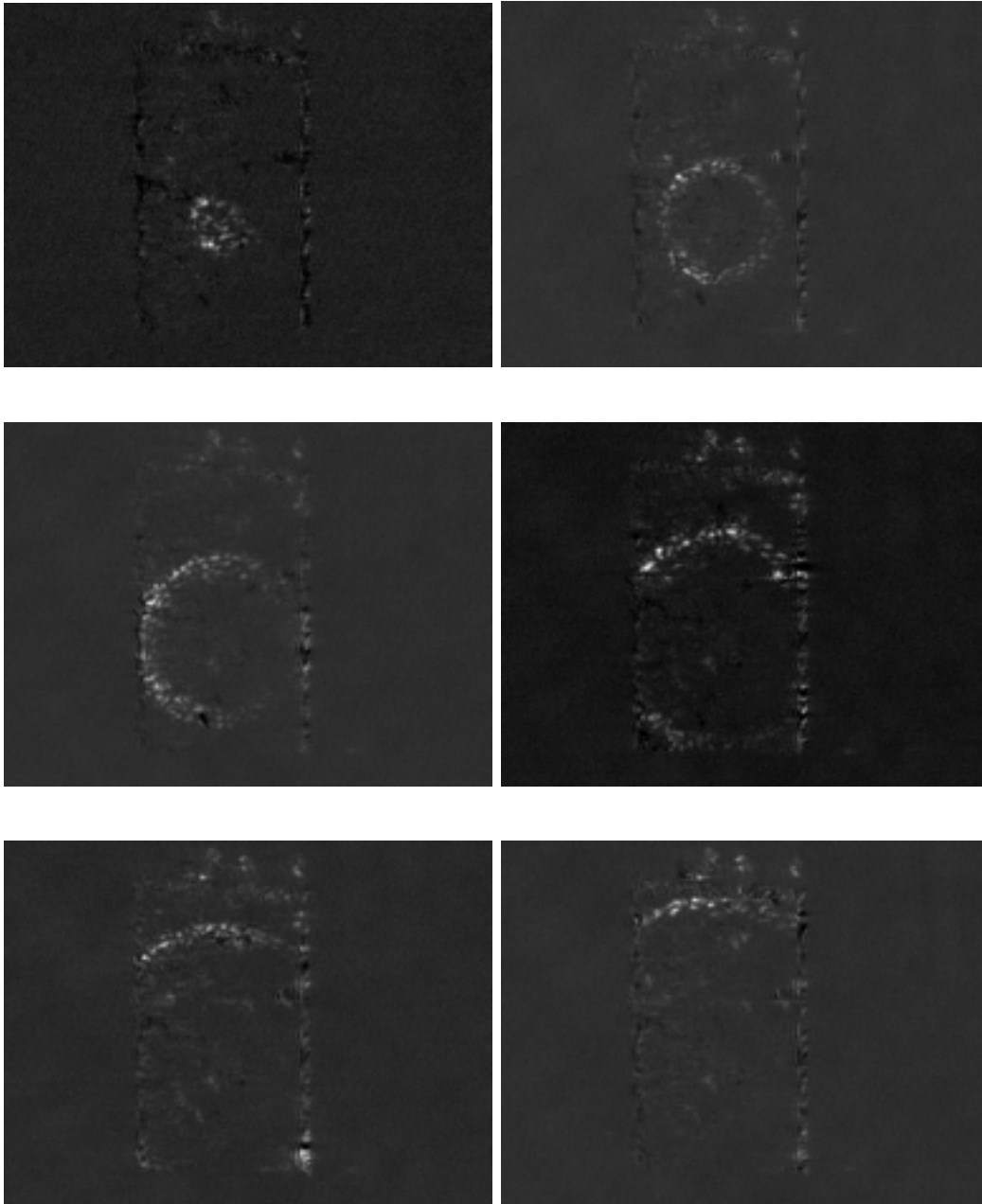


Figure 6. Holograms show 3D imaging through 3-MFP turbid medium. Other conditions are the same as figure 5. (*See electronic version for higher image quality*)

### 2.1.2 Task 1c Adaptation of the Micro-Model System for Multiphase Flow Measurements

During this reporting period, modifications were made to the micro-model flow measurement system (Figure 7) to improve our measurements of multiphase flow. Fluid pressure control is critical during the experiments because very slight pressure changes lead to large effects during drainage and imbibition. We have therefore installed more sensitive pressure transducers and have improved the pressure stability, so that ample time is available for the CCD camera to capture images of the fluid distribution.

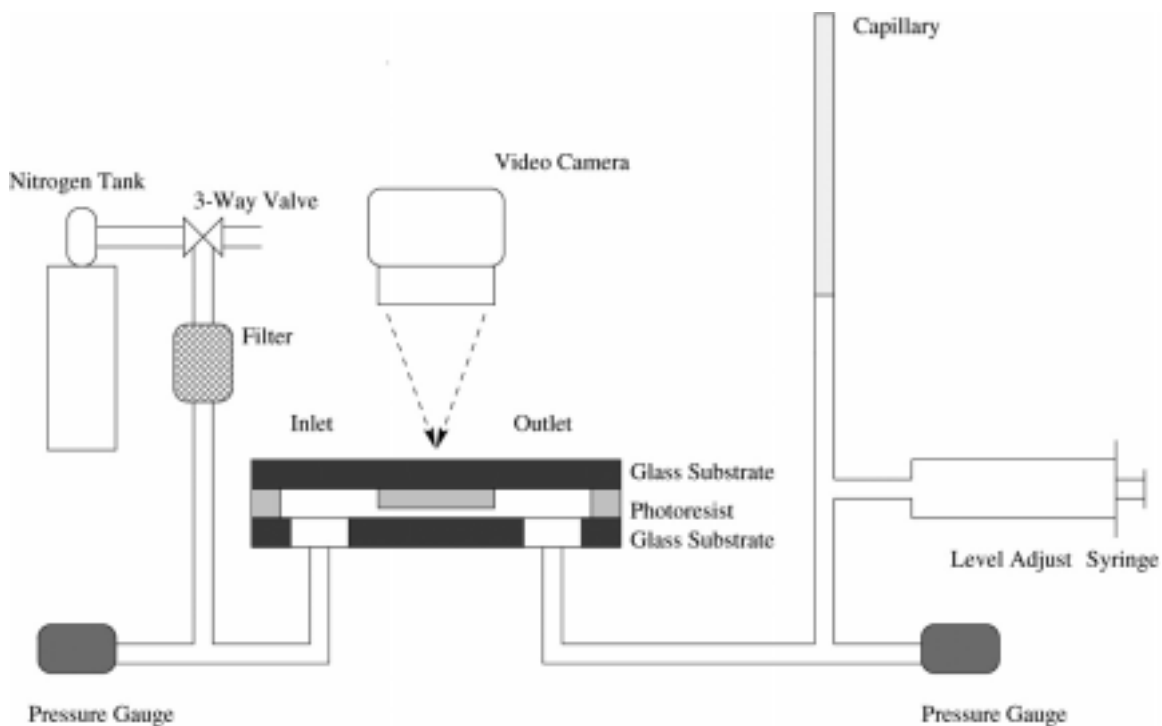


Figure 7. Sketch of apparatus for measuring and imaging multiphase flow in micro-model samples.

Additional changes to the micro-model flow system include the following. (1) Design of a new the inlet and outlet pattern, as discussed in the next paragraph. (2) Use of a new three-

way valve for the imbibition and drainage experiments. This valve enables better pressure control during flow experiments where the pressure is increased or decreased in small increments. (3) Implementation of a stainless steel filter with pore size of half micron to filter the gas. This has reduced our problems with micro-model blockage from impurities.

Figure 8 shows the new design of the inlet and outlet mask. To obtain steady-state during multiphase flow measurements, a control channel (~ 2000 microns in length) was added to the inlet and outlet mask. When performing a measurement, fluid is first introduced from the outlet. Because the control channel is long, the percolative structure (i.e., fractal pattern) can be totally saturated without completely filling the inlet channel. This insures a completely saturated micro-model which is important for the drainage experiments when gas is introduced from the inlet side. The outlet region was also modified by making it circular in shape and reducing its area. This new design facilitates the removal of gas from the percolative structure when saturating the structure from the inlet side, and reduces or eliminates residual gas in the system (for initial saturation).

### *2.1.3 Task 1d Relative Permeability/Wood's Metal Injection System*

A system for Wood's metal injection into sandstone and permeability/relative permeability measurements was designed, fabricated and constructed during the previous reporting period. During this reporting period, initial testing of the Wood's metal injection system was performed and a procedure for sample injection was developed.

The initial testing yielded the following data: (1) the length of time required to heat the Wood's metal injection system (8 hours to reach 90 °C); (2) the length of time the system is maintained at 90 °C before injection (4 hours) to insure the system and sample is thoroughly heated, and that the Wood's metal is melted; and (3) the length of that is needed for the

temperature in the tank to reach the same temperature as in outside the tank time (30 more minutes).

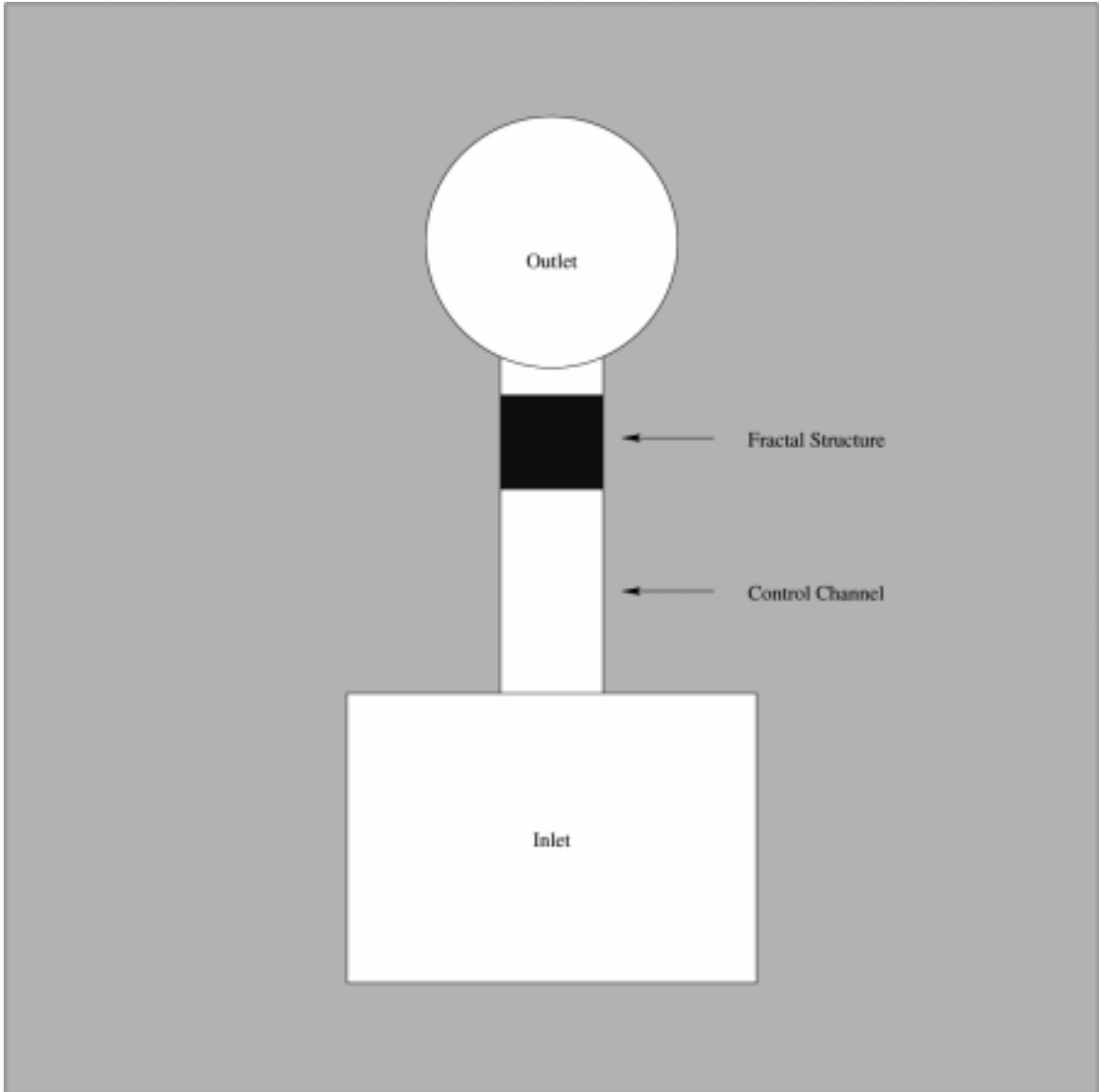


Figure 8. New design of the inlet and outlet with a control channel added.

The initial testing of the Wood's metal injection system determined the penetrated the sample and also to penetrate the porous plate and the tubing on the outlet side of the system.

The metal in the tubing solidified because the tubing was at room temperature. The solidified metal in the tubing preventing the system from reaching a steady flow condition. The system was modified to include a chamber on the outlet side of the system that is maintained at a temperature of 90 °C to prevent the metal from solidifying and to allow a steady-flow condition to be obtained. Finally, ethylene glycol was chosen as the second fluid phase that will occupy the pores during the injection and will be used for making absolute flow measurements and relative flow measurements.

Based on the initial testing of the system, the following procedure has been developed for wood's metal injection experiments:

1. Place wood's metal in Tank A (Figure 9). Mount the sample in holder and install sample in Tank C. Fill Tank C with ethylene glycol and vacuum saturate sample with ethylene glycol. Seal Tank C and fill the holding tank with paraffin oil. Close valves 1, 2, 3, 4, and 5. Place flexible heaters on the outlet tubing leading to sample and the chamber on the tubing. Monitor the temperature and pressure of the whole system.
2. Increase the temperature of the paraffin oil to 90 °C. Once a temperature of 90 °C has been achieved, maintain the temperature four hours before Wood's metal injection.
3. Apply 137.9 kPa gas pressure to Tank A. Open valves 1 and 4. Open valve 2 to let melted metal flow into Tank C until the sample is completely covered by metal as indicated by the level detector.
4. Close valves 1 and 2. Heat the outlet tubing and chamber to around 90 °C.
5. Apply desired gas pressure to Tank C. Open valves 1 and 4 for metal injection. Use scale to monitor ethylene glycol flow rate. Adjust gas pressure during the injection to maintain a constant pressure. Turn off valve 1 when steady ethylene glycol flow is reached while maintaining the pressure in Tank C. Stop heating the outlet tubing and chamber.

6. Open valve 3. Open valve 2 to let metal flow from Tank C to Tank A while the pressure in Tank C is maintained at the desired value. Let the metal flow until the sample is not in contact with the metal (based on level detector).
7. Drain paraffin oil from the holding tank and let the system to cool down.
8. Relieve gas pressure when temperature is lower than 50 °C. Open Tank C and take sample out for further experiments and measurements.

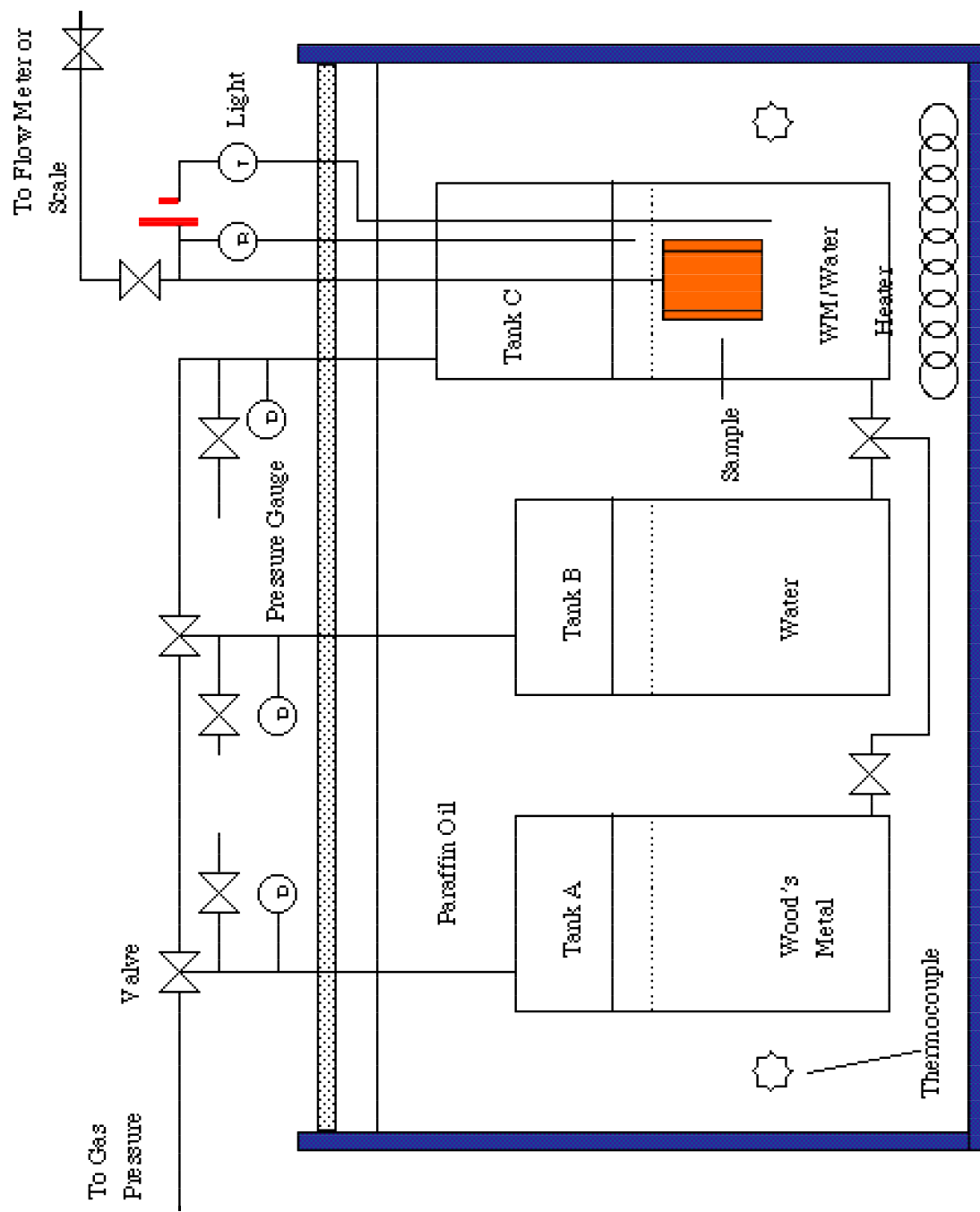


Figure 9. Schematic of Wood's metal injection system and permeability measurement system.

## 2.2 TASK 2 SAMPLE PREPARATION

### 2.2.1 Task 2a Photorefractive Quantum Well Devices (PRQW)

A new Photorefractive Quantum Well Device (PRQW) device was made that produced high quality holograms with almost no scattering centers (Figure 10). The hologram should be written with as low intensity as possible because the deeper you go into the material the less intensity will come back out. The new device showed relatively higher minimum but died quickly. It is still necessary to growth more reliable devices. A systematic study of current PRQW devices is underway to determine the properties of the PRQWs that produce the best holograms.

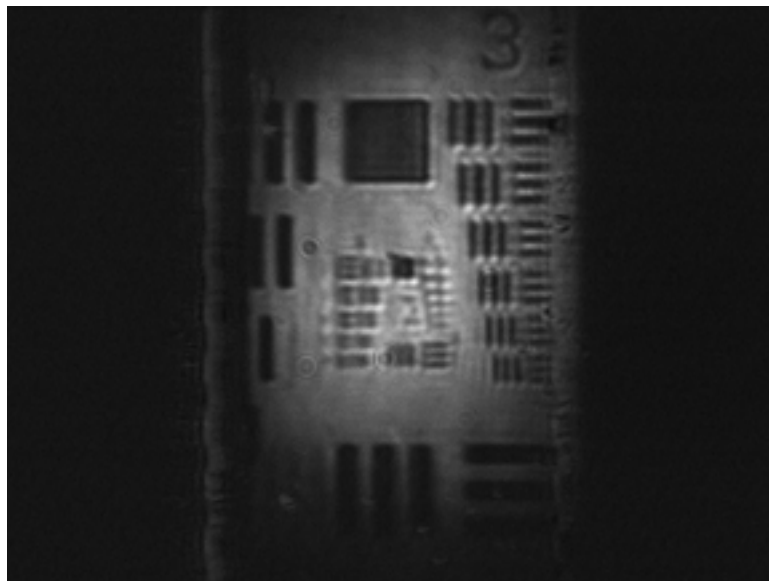


Figure 10. Holograms of the USAF test chart using a new PRQW device. (*See electronic version for higher image quality*)

### 2.2.2 Task 2b Core Samples and Boreholes

For the Wood's metal injection experiments and the permeability measurements, whole core samples from blocks of sandstone are used. A check of the uniformity of the sandstone cores is performed prior to completion of the sample processing (i.e., application of epoxy coating). The volume and weight of samples were measured and the density is calculated. To check the uniformity of the samples, the density of a sample was measured and then the sample was cut to smaller daughter and granddaughter samples and the density was measured and compared. Figure 11 shows the sample density as a function of sample volume. The result indicates that the samples have uniform density.

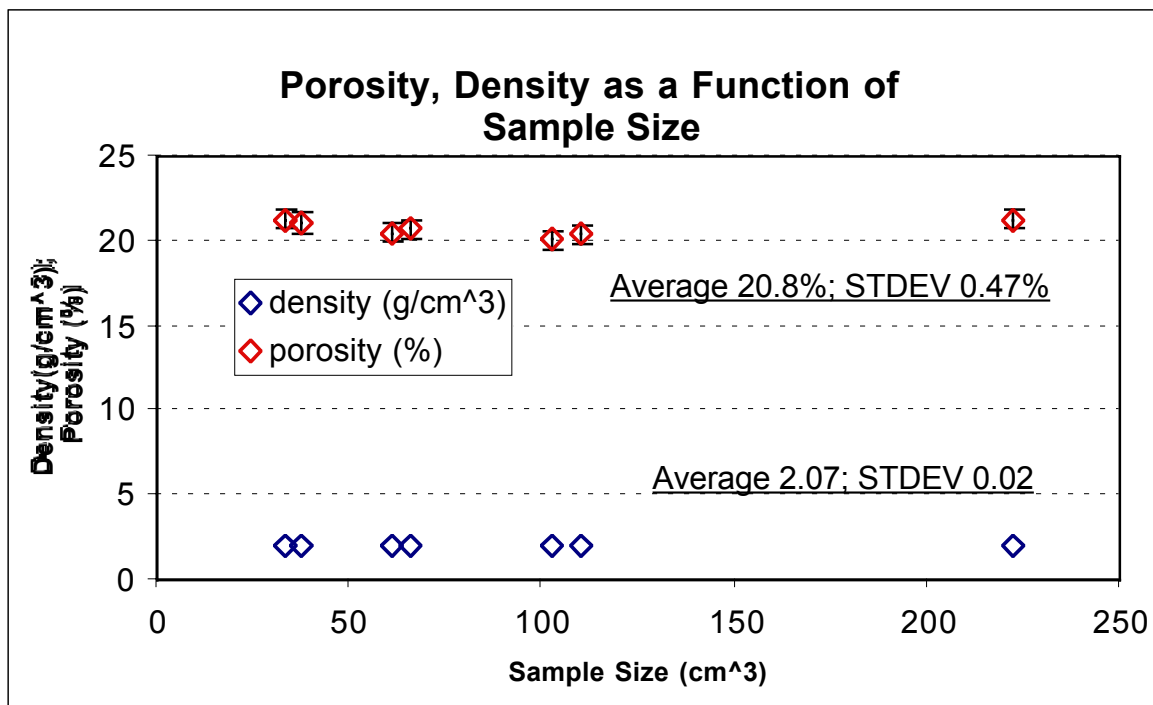


Figure 11. Sample density and porosity as function of sample size

Sample density was measured using a gas porosimeter and the wet/dry method. The gas porosimeter is home made and is base on the ideal gas law. The solid volume of the sample is measured using calipers after machining of the samples into right cylinders. In the wet/dry method, the sample is vacuum saturated and the weight difference before and after saturation is used to calculate the porosity. In Table 2, the porosity of the same samples measured by the two methods was compared. It is observed that for the samples measured, no significant difference exists. As with the sample density, the porosity of samples of different size was also compared to determine the uniformity of the sample (Figure 11). The porosity also shows that the sample is uniform. Though the values of porosity differ between the gas porosimeter and the wet/dry method, the trend in the porosity is the same for both methods. Only one method will be used for making comparisons before and after Wood’s metal injection or for comparisons among samples.

Table 2. Comparison between gas porosimeter and wet/dry porosity

Sample No.	C1	C2	C3	C4
$\phi$ (%) porosimeter	20.7	21.1	20.5	21.3
$\phi$ (%) wet/dry	20.4	20.7	20.5	21.1
Difference (%)	1.45%	1.90%	0.00%	0.94%

For the permeability and Wood’s metal injection experiments, the samples are coated with epoxy. During coating, the epoxy penetrates into the pore space that is near the surface of sample. If the volume of sample before coating was taken as the sample volume after coating, the porosity of sample decreases (Table 3). The difference in porosity (Table 3), before and after coating the sample with epoxy, is affected by the volume of pore space occupied by epoxy. As part of sample preparation, the porosity of the sample before and after coating with epoxy is measured.

Table 3. Comparison of sample porosity before and after epoxy coating

Sample No	1	2	3	4	5	6	7	8	9	10
$\phi$ (%) before coating	19.14	19.17	19.36	19.21	19.33	19.22	19.22	19.25	19.27	19.17
$\phi$ (%) after coating	18.5	18.4	19.3	16.7	18.6	16.5	18.3	18.2	18.2	18.1

### 2.2.3 Task 2c Fabrication of Micromodels

Projection photolithography is used to make percolation structures in photoresist, a light sensitive polymer). Figure 12 shows an example of a mask used to make a percolation structure micro-model for performing controlled experiments to measure absolute and relative permeability on known structures. In Figure 12, white regions represent the void space (where fluid can flow if the voids are connected) and black regions represent the grains (no flow regions). The example mask (Figure 12) was generated using a computer algorithm that is based on random continuum percolation and hierarchical cascades. The pattern in Figure 12 is called a “one tier” pattern and is a random continuum percolation pattern. If more tiers are added (Nolte et al., 1989), the spatial correlation of the void space change as well as the size of the voids (Figure 13).

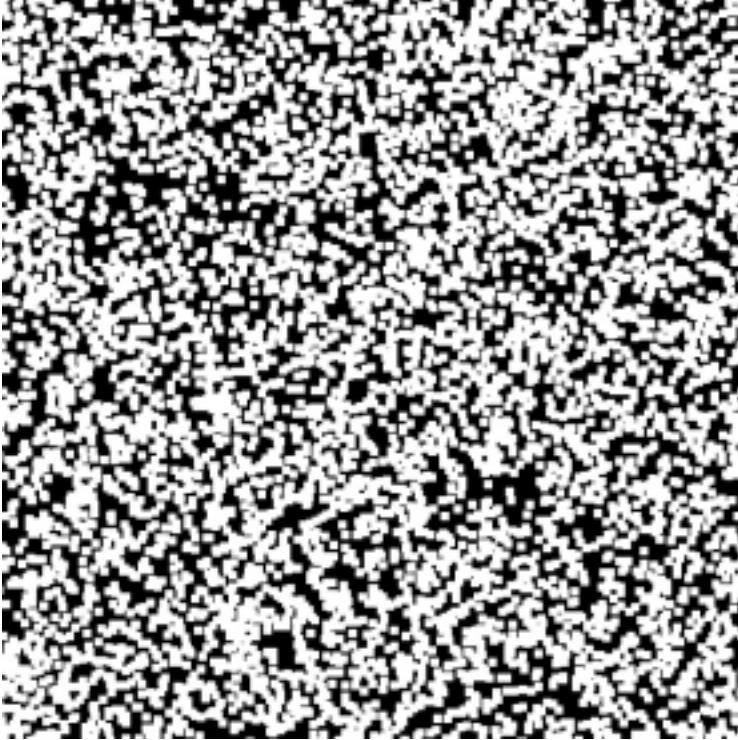


Figure 12. One tier mask used to make fractal structures.

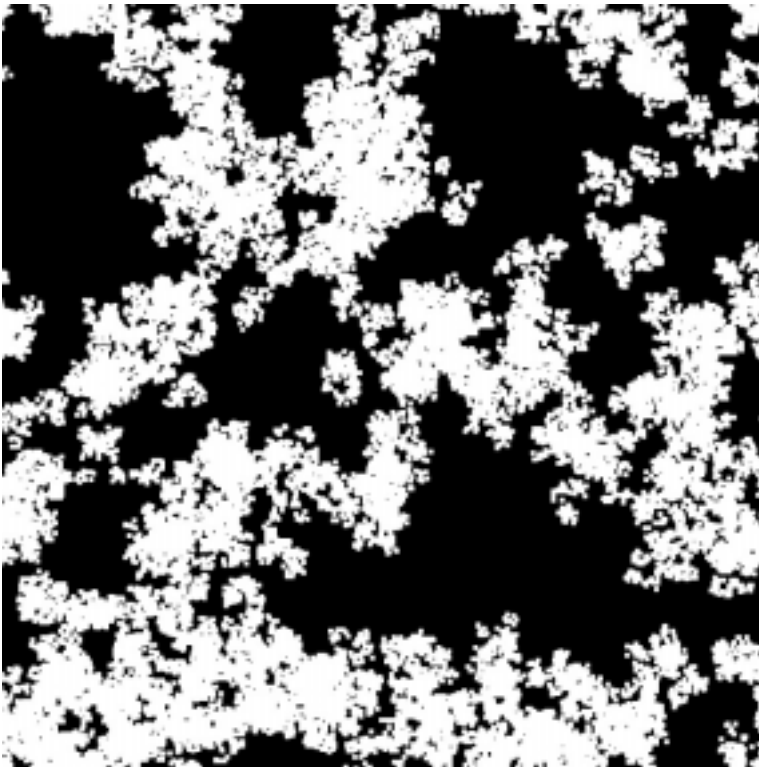


Figure 13. Five tier mask used to make fractal structures that are spatially correlated.

## 2.3 TASK 3 MEASUREMENTS OF INTERFACIAL AREA AND PORE GEOMETRY

### 2.3.1 *Task 3a Pore Geometry and Optical Coherence Imaging (OCI)*

Optical Coherence Imaging (OCI) is affected by the reflectivity of the material being probed. The reflectivity of sandstone is relatively low because of surface roughness which scatters light out of the beam. Therefore, the intensity of object arm is too weak to record the holograms. To acquire the hologram using the present settings, the sandstone sample was polished to give the sample a higher reflectivity. Figure 14 shows the direct image (Figure 14a) and hologram (Figure 14b) of polished sandstone sample. The white regions in the figure are the reflections from the surface of the grains. In the hologram, the image size is about 1.0 mm by 1.5 mm and the grains are about 30-40  $\mu\text{m}$  in size. Therefore, each grain can be resolved in our system which has resolution of 10  $\mu\text{m}$ . This data demonstrates that holograms from sandstone samples can be recorded in present system. However, only polished grains being recorded means that modifications to the OCI system, such as improvement of device sensitivity and the used of a thermally-cooled CCD camera, are necessary

### 2.3.2 *Task 3b Interfacial area, pore geometry and hydraulic properties from micro-models*

Two phase flow measurements were performed on the micro-model described in section 2.2.3. The two fluids used were nitrogen gas and silicone oil (Dow Corning 200 Fluids, 100 cs). Silicone oil was selected because its surface tension is only one third that of water (71.69 mN/m for water at 25 °C). Some properties of the silicone oil are listed in Table 5.

Initial tests performed with water (in place of silicone oil) showed that residual air in the water would cause air bubbles to form in the sample, and this made precise imaging extremely difficult. Good image quality is needed to quantify the distribution of each fluid

phase and other geometric properties such as interfacial area per volume to test upscaling theorems.

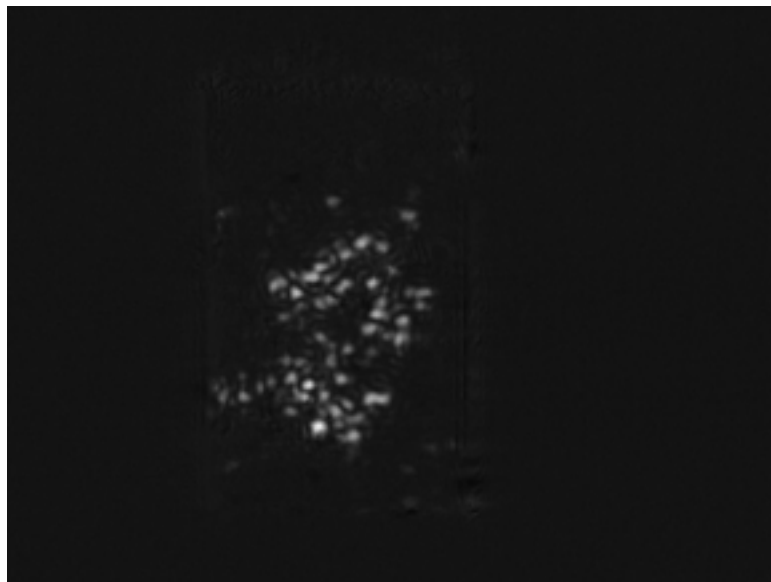
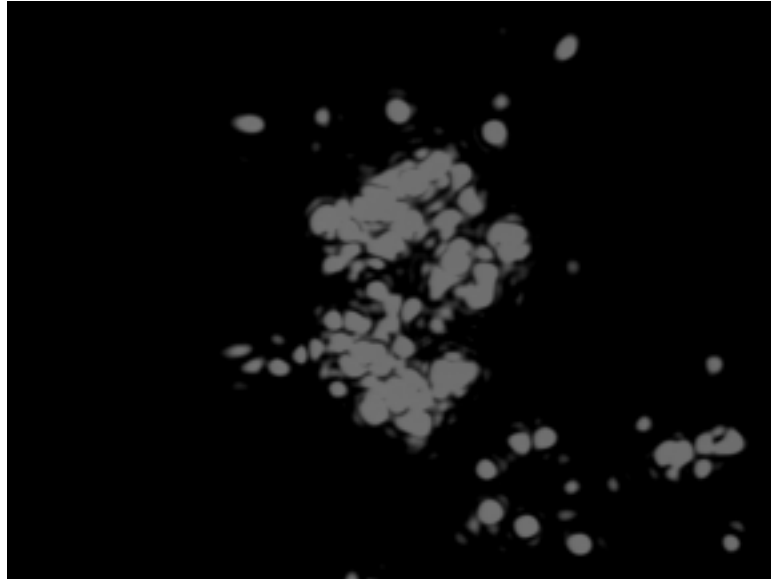


Figure 14. Direct image (a) and hologram (b) of polished sandstone. The hologram has a size of  $1.0 \times 1.5 \text{ mm}^2$  and resolution of  $10 \text{ }\mu\text{m}$ . The white region corresponds to grains which are  $30\text{-}50 \text{ }\mu\text{m}$  in size. (*See electronic version for higher image quality*)

Table 4. Properties of Silicone oil.

Specific gravity	0.964gm/ml
Surface tension	20.9 mN/m
Viscosity	101.8 cp

Figure 15 is an image of the micro-model that was fabricated with the mask described in section 2.2.3. The pore depth (aperture – height perpendicular to the page) is  $1.0 \pm 0.1\mu\text{m}$ . Results of a typical measurement are shown in Figure 16. Here the micro-model in Figure 15 was first filled with silicone oil, and then nitrogen gas was introduced from the edge of the sample at the top of the figure. This gas displaced oil as it penetrated, and the amount of area filled with gas increased as the gas pressure was increased. Eventually, the gas region penetrated to the bottom edge of the sample, so that gas could then flow through the entire sample, and imbibition was complete. At that point the pressure was decreased so that the complementary process of drainage could be studied. The picture in Figure 16 was taken during the drainage process; it can be seen that a gas filled region does not now extend through the sample, and that many pockets of gas have become isolated within the oil.

Figure 17 shows a typical imbibition / drainage cycle for a sample like the micro-model shown above. With the accessible pore space initially filled with oil, nitrogen gas was then injected, initially at a low pressure. As this pressure was increased, the gas penetrated and the area of the wetting fluid (i.e., oil) decreased; this is the bottom branch of the curve in Figure 17. As the pressure was increased further, one moves to the left along this branch, as the wetting fluid saturation continues to decrease. As noted above in connection with the

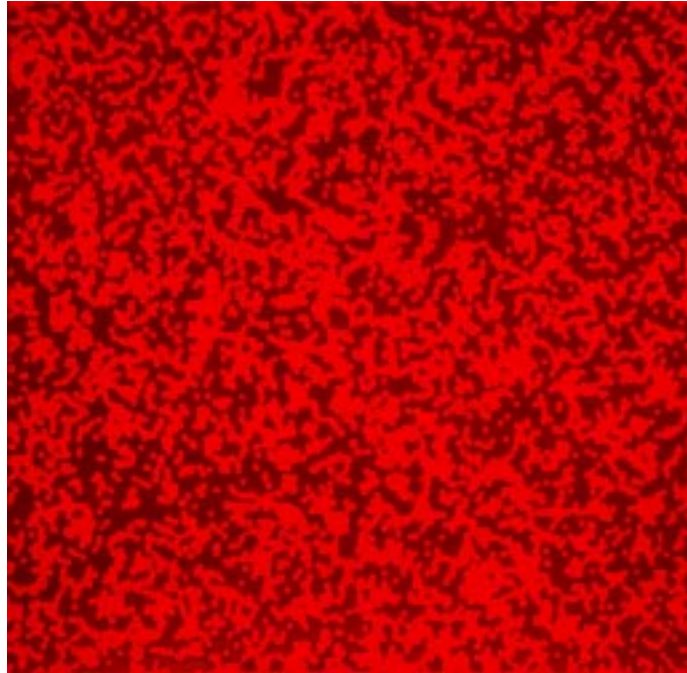


Figure 15. Using the mask shown in Figure 12, we made a micro-model with this percolation geometry. The pattern was taken in red light to prevent unwanted photochemical reactions in the photoresist layer in which the pattern is etched. The region shown here is 600 micron long and wide. The darker area is photoresist, and the brighter area is void space.

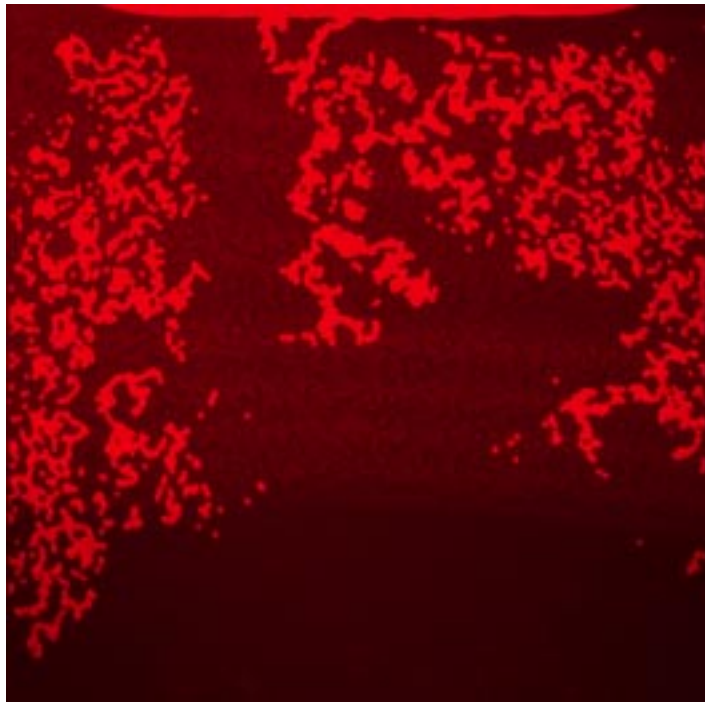


Figure 16. A fractal micro-model filled with silicone oil and nitrogen gas. The brightest region is gas and the darker regions show the space filled with silicone oil and the inaccessible regions (compare with Figure 15, which shows the same micro-model with an empty void space).

discussion of Figure 16, the gas eventually penetrates across the sample and flow begins; this occurred at the upper right corner in Figure 16. When the pressure was then decreased the upper curve (labeled drainage) was followed, as the area of the wetting phase now increased. The precise imbibition/drainage curve was found to be a sensitive function of the speed at which the pressure was varied. In Figure 17, the pressure was increased slowly (a few minutes between each data point) and the system was allowed to equilibrate for at least one minute prior to each measurement. If the pressure was increased more rapidly a completely different curve was observed. Hence, not surprisingly, the dynamics of imbibition and drainage plays a key role.

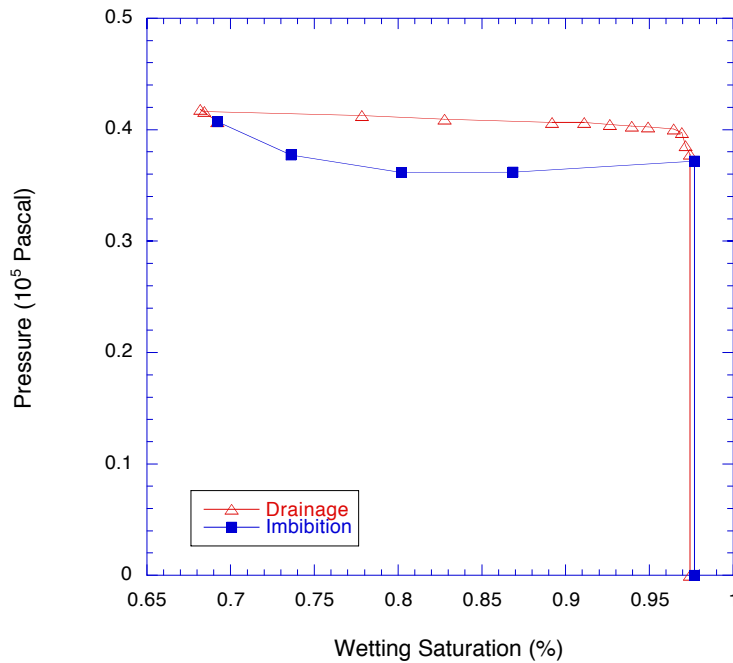


Figure 17. Drainage and imbibition curve for silicone oil / nitrogen gas in the micro-model shown in Figure 16. The horizontal axis gives the fraction of the available pore area which is occupied by the wetting phase (oil).

### 2.3.3 Task 3c Interfacial area, pore geometry and hydraulic measurements on Core samples

During this reporting period, initial measurements of gas, water and/or ethylene glycol absolute permeability were made. All of these measurements were conducted under room temperature conditions. A study of the repeatability of the measurements was performed. Nitrogen ( $N_2$ ) was used for the gas permeability tests. Figure 18 shows the flow rate versus gas pressure of two trials of measurement on the same sample. The results indicate a linear relationship between flow and pressure for the range of pressures used in the tests and repeatable results.

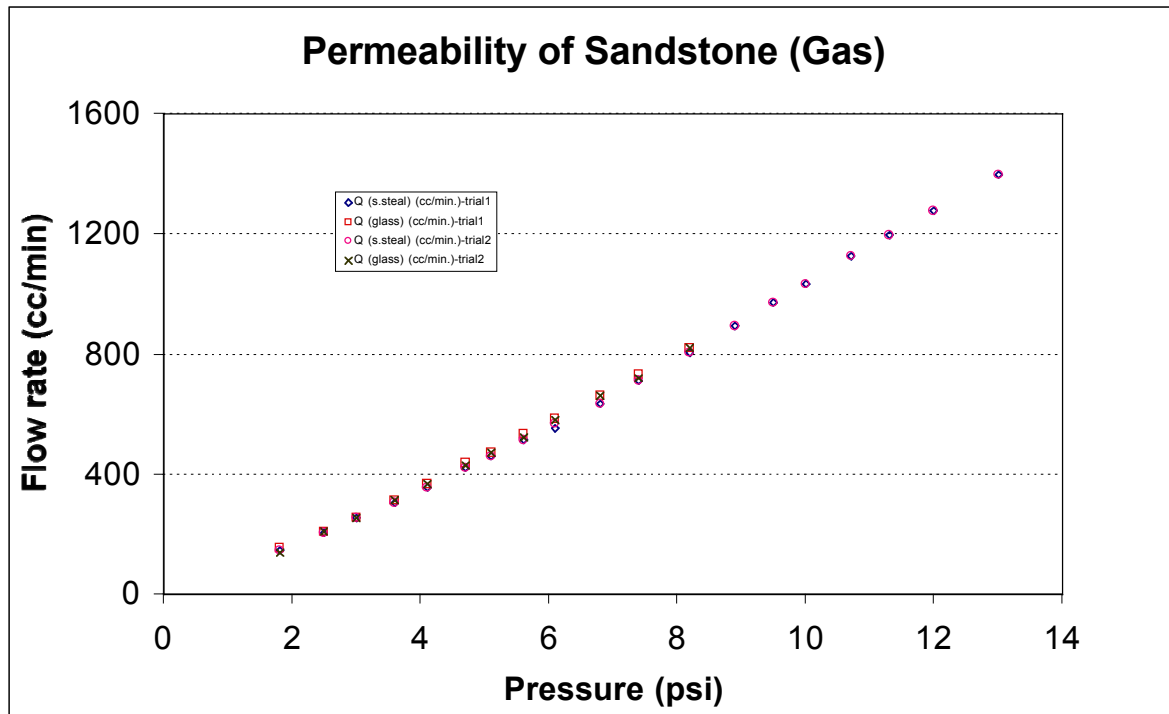


Figure 18. Flow rate versus gas pressure during gas permeability measurement.

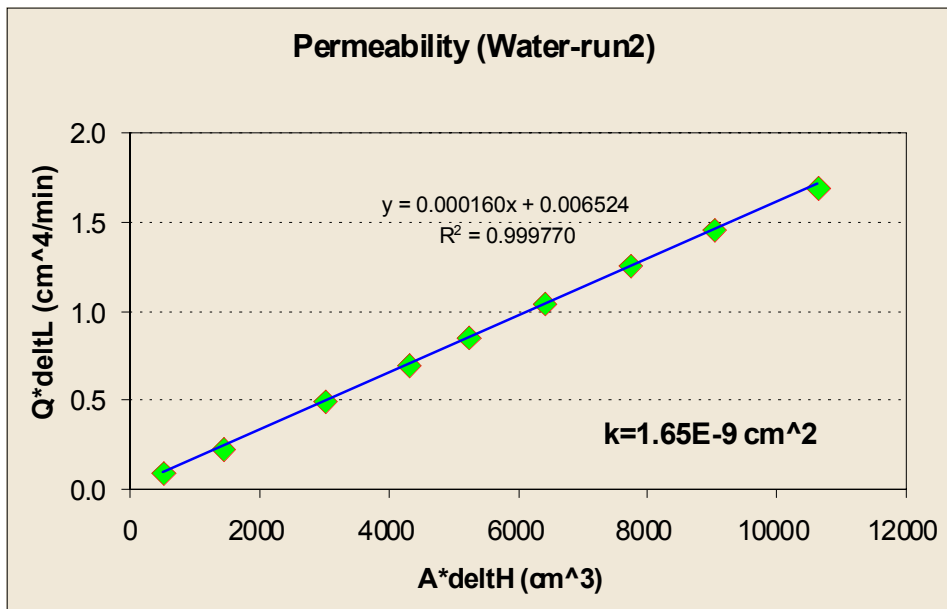
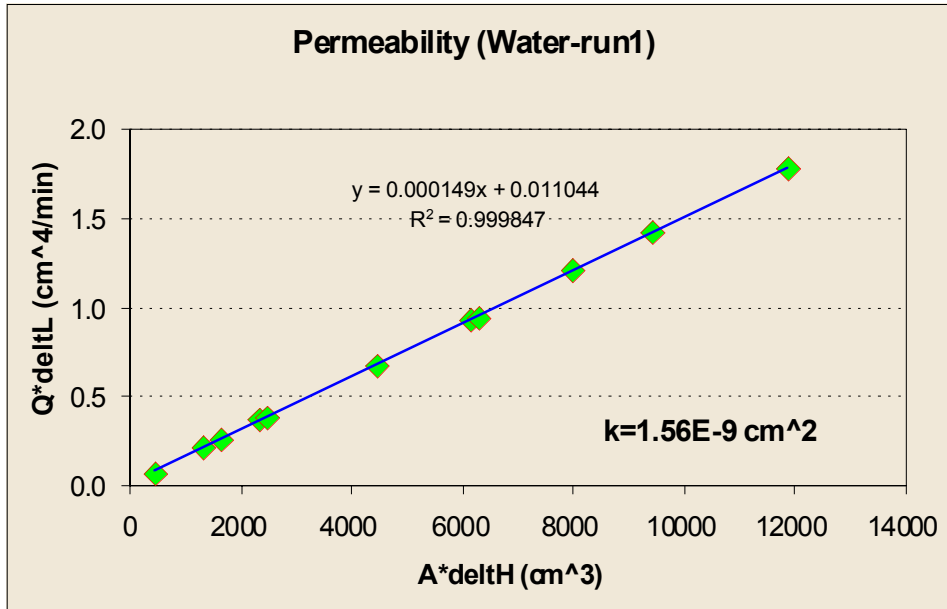


Figure 19. Water flow rate versus gas pressure during gas permeability measurement for Run 1 and Run 2. Units are converted and the slope of the fitted line is the permeability in unit of L/T<sup>2</sup>.

Figure 19 contains the results of absolute water permeability measurements made on the same sample as the gas flow measurements. The sample was dried after the first measurement

and re-saturated with water before the second measurement. The permeability was  $1.56 \times 10^{-9}$   $\text{cm}^2$  and  $1.65 \times 10^{-9}$   $\text{cm}^2$ . The percent difference is 5.4%.

A portion of this task is dedicated to imaging the pore structure in the sandstone samples, as well as geometry of the fluid phases that occupy the pores. During this reporting period, initial tests for imaging the pore space were performed on a Wood's metal injected sample of sandstone. When an injected sample was cut, the wood's metal smeared on the cut surfaces. The deformation of Wood's metal caused problems in constructing the pore geometry from photographs of the surfaces (Figure 20). Another problem is that the images are not easy to be analyzed/processed because it is difficult to distinguish wood's metal and some sand grains. The proposed solution to the problem of the deforming Wood's metal (smearing metal) during cutting is to epoxy inject the sample before cutting. Injected epoxy will occupy the pore spaces not reached by the metal and therefore the metal will not be deformed (or smeared) during cutting. In addition, instead of using an optical microscope to image the pore space, it is proposed to use a Scanning electronic microscope (SEM) to improve the quality the images.

### **3.0 Conclusions and Future Work**

#### **3.1 OPTICAL COHERENCE IMAGING**

The OCI system was modified to obtain a resolution of  $10 \mu\text{m}$  and improve the intensity of the images (16 times compared to previous system). Holograms were acquired from an USAF test chart through 6-MFP turbid medium. The results show that the system receives images from "ballistic" light from the sample and rejects scattered light from turbid medium. The work performed also demonstrates the ability of OCI to do laser ranging by coherent imaging to acquire three-dimensional information. Holograms of the surface of polished

sandstone were recorded successfully. In future, we will increase the system sensitivity by growth of more sensitive PRQW devices and through the use of a thermally-cooled CCD camera. Future work also includes performing laser ranging on sandstone samples and work to image through one layers of grains.

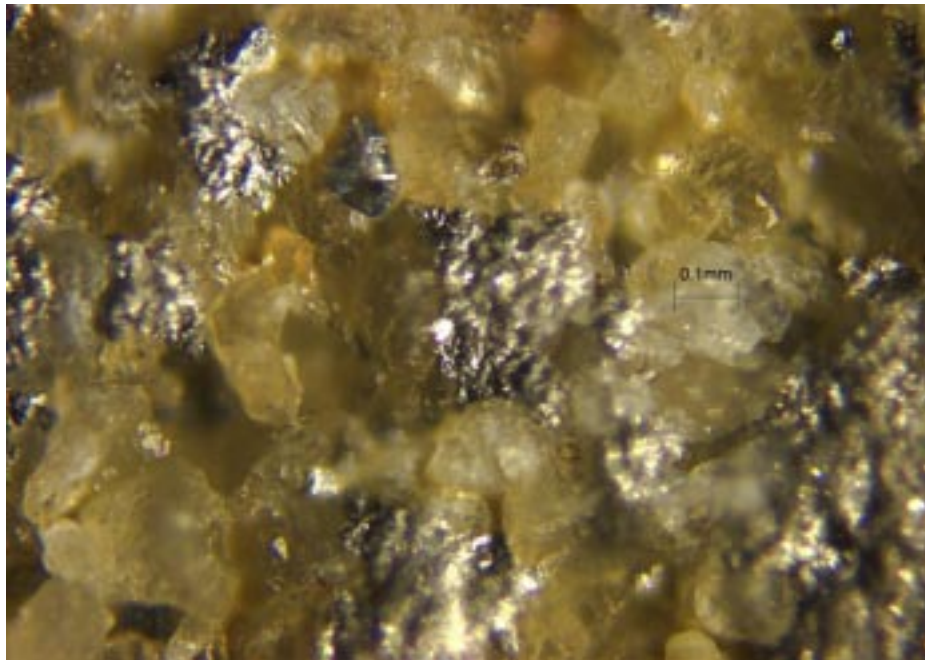


Figure 20. Image of Wood's metal injected sandstone obtained using an optical microscope.

### 3.2 MICRO-MODELS

We have established that our improved apparatus and micro-model design now permit detailed studies of fluid motion and behavior. Our next job is to undertake detailed measurements, similar but more extensive than those shown in the figures above, to study the behavior of a wide range of micro-models. These will include regular pore geometries, fractal structures like the one shown above, and geometries obtained from the Woods Metal

work on real porous materials. Our image quality is now quite good, and will enable us to measure the interfacial area between the two fluid phases, so that the full three dimensional phase space of capillary pressure – saturation – interfacial area can be explored in detail. It will be important if the behavior can be described by a single surface in this three dimensional space, or if the nature of this surface depends on other variables such as the rate of pressure increase or decrease.

Another near-term objective will be to develop a method for fabrication of multi-layer flow micro-models. This will allow us to extend our work to structures which are more nearly three dimensional, and are thus more representative of real materials.

### 3.3 WOOD'S METAL INJECTION

A system for Wood's metal injection and permeability measurements was constructed and initial tests were performed. A procedure for Wood's metal injection of sandstone cores was developed. Initial testing of the permeability portion of the system was also tested and found to be repeatable. In addition, initial tests on imaging the pore geometry of metal injected samples produce images of insufficient quality to produce reliable data. During the next period, the procedure for obtaining high quality images of the pore space geometry will be developed and involve (1) epoxy injection of the Wood's metal injected sample prior to cutting; (2) polishing of the epoxy & Wood's metal injected sample; and (3) using a Scanning Electron Microscope for capturing the images. In addition, during the next reporting period, several ethylene glycol saturated samples will be injected with Wood's metal at different capillary pressures and ethylene-glycol flow rates before and after Wood's metal injection will be made. These experiments will provide data on the effect of fluid phase distribution in the pore space of sandstone on relative permeability measurements.

#### 4.0 References

- Darcy, H., Determination of the laws of flow through sand, Les fontaines publiques de la ville de Dijon, Victor Dalmont, Paris, 1856, 590-594, (translated and reprinted in Physical Hydrology, edited by R. A. Freeze and W. Back, Hutchinson Ross Publishing Company, Stroudsburg, PA, 1983).
- Gray, W. G., General conservation equations for multi-phase systems: 4. Constitutive theory including phase change, *Adv. Water Resources* 6, 130-140 (1983).
- Gray, W. G. (private communication, 1998).
- Hassanizadeh, S. M. and W. G. Gray, General conservation equations for multi-phase systems: 1. Averaging procedure, *Adv. Water Resources* 2, 131-144 (1979).
- Hassanizadeh, S. M. and W. G. Gray, Mechanics and thermodynamics of multiphase flow in porous media including interphase boundaries, *Water Resource Research*, 13, 169-186 (1990).
- Kalaydjian, F., Origin and quantification of coupling between relative permeabilities for two-phase flow in porous media, *Transport in Porous Media* 5, 215 (1990).
- Muccino, J. C., Gray, W. G. and L. A. Ferrand, Toward and improved understanding of multiphase flow in porous media, in press, *Rev. Geophys.* (1998).
- Nolte, D.D., Pyrak-Nolte, L.J., and N.G.W. Cook, 1989, Fractal Geometry of the Flow Paths in Natural Fractures and the Approach to Percolation, *Pure and Applied Geophysics*, Vol. 131, no. 1/2, p.111.